Groundwater Flow Monitoring via Combined Time-lapse Electrical Resistivity and Self Potential Data Tomography

Lige Bai[1], jing li[1], Li Guo[2], Hui Liu[1], Jiawei Tan[1], and Tianqi Wang[1]

[1]Jilin University
[2]Pennsylvania State University

May 26, 2020

Abstract

Revealing the dynamics of groundwater movement in the vadose zone is crucial to groundwater management and artificial recharge. The traditional hydrographic surveys are usually indirect, costly, and infrequent. In this study, the groundwater flow characterization of a pumping experiment in Jilin University campus was monitored through combining time-lapse electrical resistivity tomography (ERT) and self-potential (SP) data tomography. The ERT datum depicts the spatial distribution of resistivity, which is related to the dynamics of soil moisture content during the pumping process. We are able to correlate hydraulic heads and SP signal during a decline and recovery groundwater level period leading to interesting perspectives in understanding the dynamics of complex groundwater flow. The SP method provides a direct way to estimate the potential field distribution, which can be further used to invert soil permeability. A total of 24 hours of time-lapse geophysical surveys revealed a significant increase in resistivity but a decrease in permeability during water pumping and groundwater recharge, representing the process of groundwater decline and recovery. Results derived from time-lapse geophysical surveys matched well with in situ monitoring of the groundwater level. The study demonstrates that the combined ERT and SP data can provide a direct and reliable way to monitor groundwater flow or other time-lapse hydrogeological surveys.

Groundwater Flow Monitoring via Combined Time-lapse Electrical Resistivity and Self Potential Data Tomography

Lige Bai[1], Jing Li[1*], Li Guo[2,3], Hui Liu[1], Jaiwei Tan[1], Tianqi Wang[1]

[1] College of Geo-exploration Sci. &Tech, Jilin University, Changchun, Jilin 130026, China

[2] State Key Laboratory of Hydraulics and Mountain River Engineering, College of Water Resource and Hydropower, Sichuan University, Chengdu 610065, China

[3] Department of Ecosystem Science and Management, Pennsylvania State University, University Park, PA 16802, USA

*Corresponding author: Jing Li,*inter.lijing@gmail.com*

Key words: Groundwater Flow Monitoring; Time-lapse; Electrical Resistivity Tomography (ERT); Self-potential (SP) Tomography

Funding Information: This work are supported by the Natural Science Foundation of China (41874134), the Jilin Excellent Youth Fund (20190103142JH) and the China Postdoctoral Science Foundation 2015M571366

Summary

Revealing the dynamics of groundwater movement in the vadose zone is crucial to groundwater management and artificial recharge. The traditional hydrographic surveys are usually indirect, costly, and infrequent. In

this study, the groundwater flow characterization of a pumping experiment in Jilin University campus was monitored through combining time-lapse electrical resistivity tomography (ERT) and self-potential (SP) data tomography. The ERT datum depicts the spatial distribution of resistivity, which is related to the dynamics of soil moisture content during the pumping process. We are able to correlate hydraulic heads and SP signal during a decline and recovery groundwater level period leading to interesting perspectives in understanding the dynamics of complex groundwater flow. The SP method provides a direct way to estimate the potential field distribution, which can be further used to invert soil permeability. A total of 24 hours of time-lapse geophysical surveys revealed a significant increase in resistivity but a decrease in permeability during water pumping and groundwater recharge, representing the process of groundwater decline and recovery. Results derived from time-lapse geophysical surveys matched well with *in situ* monitoring of the groundwater level. The study demonstrates that the combined ERT and SP data can provide a direct and reliable way to monitor groundwater flow or other time-lapse hydrogeological surveys.

1 Introduction

Knowledge of groundwater flow and groundwater level variation is crucial to groundwater management and water quality control (Tesfaldet et al., 2019). A better understanding of the mechanism governing groundwater movement in the vadose zone requires investigations on both groundwater flow characterization and the recharging process (Nielsen et al., 1986). Traditional hydrographic groundwater surveys include float, pressure, and automatic tracking observations. However, when measuring the dynamics of the groundwater level over a long period, the measurement is usually indirect, costly, and infrequent (Ogilvy et al., 2009). In contrast, the nonintrusive time-lapse geophysics tools provide an opportunity to complement traditional measurements (Fetter, 2001), especially given that geophysical surveys can be implemented over a large region with dense sampling intervals in both space and time. In particular, electrical resistivity tomography (ERT) and self-potential (SP) tomography are appropriate to monitor groundwater dynamics due to the sensitivity of resistivity and apparent current density to changes in flow or water chemistry (Carey, 2017; Revil & Linde, 2006). The time-lapse method carries out periodic measurements at a fixed location and determines the 2D/3D groundwater flow by analyzing the response variation in the subsurface over a specific period (Doetsch et al., 2012).

The ERT is sensitive to changes in pore water electrical conductivity and temperature. Therefore, it has been used to track the subsurface migration of conductive tracers and image the hydraulic conductivity of heterogeneous aquifers (Bowling et al., 2006). The time-lapse ERT method has been well established for soil moisture estimation and groundwater flow monitoring (Jongmans & Garambois, 2007; Niesner, 2010). It measures the resistivity of the subsurface by using an electrode dipole to inject direct current into the ground and using additional dipoles to measure the resulting voltage. Many studies have explored the challenges and uncertainties associated with predicting groundwater flow using ERT. However, for small-scale groundwater flow, there is not apparent resistivity change, and the ERT is not sensitive to describe the groundwater movement (Fagerlund and Heinson, 2003). The SP method is used to monitor the groundwater based on its flow characteristic. The SP signal has two main components: (1) the electrokinetic contribution associated with groundwater flow through the permeable soil and (2) oxide-reduction phenomena (Naudet et al., 2003). Sill (1983) used physical approaches to simulate the SP anomalies related to groundwater flow by solving the constitutive equation corresponding to groundwater flow. By observing the SP data on the ground surface, both potential and current density distributions of the underground space can be effectively calculated to quantify the abnormal distribution characteristics. In recent years, the application of the geophysics potential method in the inversion of geophysical parameters, such as changes in the hydraulic head using SP technology to reconstruct pumping tests, has attracted increasing attention (Revil & Linde, 2006).

The ERT and SP methods have different physical mechanisms to describe groundwater flow characterization. ERT utilizes the change of resistivity caused by the variations of moisture content in the soil, while the groundwater movement produces the SP signal. Combining the two methods for cross-validation will provide a more robust result (Fan et al., 2020; Guo et al., 2020). This study addressed two primary questions: 1)

What is the advantage of the combined time-lapse strategy; and 2) How does the magnitude and timing of water input change groundwater flow dynamics? To answer these questions, we propose the combined ERT and SP method strategy to monitor the groundwater flow variation in a pumping experiment. The groundwater level is controlled by pumping water from shallow water well to create various conditions of groundwater flow. The time-lapse ERT data can be used to derive the dynamics in resistivity distribution, which reflects the evolution of soil moisture content over time. Then, the SP data and ERT result can be combined to invert the resistivity and estimate the permeability distribution. The proposed method was tested in a pumping experiment, and the geophysical results agreed well with direct monitoring of the groundwater level in wells. The results of this study provide a reliable and low-cost way to identify and monitor the groundwater movement in the vadose zone.

2 The Self-potential Inversion Theory

Self-potential (SP) refers to passively measure electric potentials that are generated through coupling with some other forcing mechanism, which is often hydraulic, chemical, or thermal. This coupled flow mechanism in this stratigraphic setting was detected on the surface by Minsley, (2007). Over the years, there has been a growing interest in the application of the SP method in various fields of earth science, including hydrology, geothermal and geotechnical and environmental engineering (Darnet& Marquis, 2004). In many cases, this method is relatively easy to use and convenient for qualitative interpretation. In this section, we present the forward and inverse theory of the SP method. Meanwhile, the permeability tensor can be determined directly according to the coupling coefficient. The problem can then be solved independently by resistivity tomography.

2.1 Forward Modeling

Use the constitutive equation to explain the hydraulic problems of heterogeneous and anisotropic porous materials:

$$\begin{cases} a\frac{\partial h}{\partial t} + \nabla \bullet \mathbf{u} = Q_{\mathbf{s}} \\ \mathbf{u} = -K\nabla h \end{cases} \quad (2.1)$$

Where h denotes the hydraulic head (in m), $a(\mathrm{m}^{-1})$ denotes the storage ratio, Qs denotes the external sources, $\mathbf{u}$ denotes the Darcy velocity ($\mathrm{m}\bullet\mathrm{s}^{-1}$), and $K(\mathrm{m}\bullet\mathrm{s}^{-1})$ means the penetration rate. The pressure of pore fluid p (in pa) can be expressed as the relationship between the mass density of pore water (in $\mathrm{kg/m}^3$), the acceleration of gravity g (in $\mathrm{m/s}^2$), and the hydraulic head h (in m) p=$\rho_{\mathbf{f}} g(h-z)$. $\mathbf{z}$ (in m) is the constant elevation above a given datum. Eq 2.1 should follow the first type boundary (Dirichlet) condition and the second type boundary (Neumann) condition while following the initial term.

Boundary {

$$\begin{matrix} h = h_D \text{ at } \Gamma_D \\ -nK\nabla h = q_0 \text{ at } \Gamma_N \end{matrix} \quad \textit{(2.2)}$$

Initial $h = h_0$ *at* $t = 0$ *(2.3)*

After solving hydraulic problems, it is essential to analyze electrical problems. The sum of conductive current density (Ohm's Law)$-\sigma\nabla\psi$ and the current source density$\mathbf{j}_s$is the total current density $\mathbf{j}(\mathrm{A/m}^2)$ (Ahmed &Jardani, 2013).

$$\mathbf{j} = -\sigma\nabla\psi + \mathbf{j}_s \quad (2.4)$$

$$\mathbf{j}_s = Q_V\mathbf{u} \quad (2.5)$$

Where ψ (in V) denotes the electrical potential, σ is the electrical conductivity tensor. Q_V is the effective excess charge density tensor of the pore water per unit pore volume.Q_V can be predicted from the permeability tensor according to (Jardani et al., 2007):

$$\log_{10} Q_V = -9.2 - 0.82 \log_{10} K \quad (2.6)$$

According to the continuity equation of charge$\nabla \mathbf{j} = 0$:

$$\nabla \bullet (\sigma \nabla \psi) = \nabla \bullet \mathbf{j}_s (2.7)$$

Where a Neumann boundary condition Γ_{NV} is applied to the upper interface (air-ground) and a Dirichlet boundary condition Γ_{DV} is used to other boundaries. It can ensure that the response of the underground potential is received on the ground surface. The boundary problem indicates that the anomaly contains some information related to the hydraulic flow path (Revil et al., 2010).

2.2 Inverse Problem

Source inversion is an ill-posed, non-unique problem that can be solved by incorporating model regularization into the inverse problem. According to the SP inversion method proposed by Ahmed and Jardani (2013), the spatial distribution of potential anomalies caused by the underground current density vector is obtained by M:

$$\psi(N) = \int_{\Omega} G(N, M) \mathbf{j}_s(M) \, \mathrm{dV} \quad (2.8)$$

Where $\mathbf{j}_s(M)$ is the current density source at a set of points M, $\psi(N)$ is the potential at a set of N electrodes, and$G(N, M)$ represents the measured natural potential data at point N and is currently at point M Kernel matrix. The calculation of the $G(N, M)$ kernel function depends on the selection of two parameters: 1) the conductivity value of the medium; 2) the number of discrete elements M. The kernel matrix can be solved by using the finite element method (Trujillo-Barreto et al., 2004).

$$\phi_d = \left\| W_d (G\omega - \psi^{\mathrm{obs}}) \right\|_2^2 (2.9)$$

$$\psi^{\mathrm{obs}} = [\psi_1^{\mathrm{obs}}, \psi_2^{\mathrm{obs}}, \psi_3^{\mathrm{obs}}, \ldots, \psi_N^{\mathrm{obs}}]^T (2.10)$$

$$W_d = diag[\tfrac{1}{\delta_1}, \tfrac{1}{\delta_2}, \ldots, \tfrac{1}{\delta_N}] (2.11)$$

Where $\|\|_2$ is the L2 norm, G represents the kernel matrix of N x $2M$ (corresponding to the self-potential measured at each site), and ω is the current density j_s related to the potential and the kernel matrix G.ψ^{obs} denotes a vector of N elements corresponding to a set of self-potential data, W_d is an N x N diagonal weighted square matrix, and δ_1 denotes the square of the deviation (Linde et al., 2007). Because the inversion leads to ill-posedness of the solution, a regularization term, and a depth weighting function ϕ_m are added to the analysis process to reduce the problem of overfitting. Establish the global objective function term ϕ_T (Menke, 1984):

$$\phi_T = \phi_d + \phi_m = \left\| W_d (G\omega - \psi^{\mathrm{obs}}) \right\|_2^2 + \lambda^2 \left\| W_m (\omega - \omega_0) \right\|_2^2 (2.12)$$

$W_m = LW_z = (z_0 + z)^{-\frac{\beta}{2}}$ denotes a depth-weighted matrix of N x $2M$ (Li & Oldenburg, 1998),z_0 denotes the observation height of the model unit, and $L$is the smoothness based on the first derivative of ω, $\beta$is a constant term between 1 and 4. λ denotes the regularized constraint term 0 <λ <[?], and the objective function of the above formula is in the standard form:

$$\phi_T = \left\| G\omega - \psi^{\mathrm{obs}} \right\|_2^2 + \lambda \left\| \omega - \omega_0 \right\|_2^2 (2.13)$$

Where$G$,ω,ψ^{obs},and $L_P$are matrices deduced by the Elédn's algorithm based on QR decomposition (Elédn, 1977). The solution to finding the minimum value of the objective function ϕ_T (Hansen, 1998):

$$min(\left\| G\omega - \psi^{\mathrm{obs}} \right\|_2^2 + \lambda \left\| \omega - \omega_0 \right\|_2^2) (2.14)$$

$$\hat{\omega}(\lambda) = [G^T G + \lambda E]^{-1} (G^T \psi^{\mathrm{obs}} + \lambda \omega_0) (2.15)$$

When the permeability is known, the current density distribution can be calculated for the prior model of the objective function, and in the case where there is no prior information, we assume the model$\omega_0 = 0$:

$\hat{\omega}(\lambda) = [G^T G + \lambda E]^{-1} G^T \psi^{\text{obs}}$ (2.16)

The singular value decomposition (SVD) method is used$G = \sum_{i=1} u \Lambda v^T, = min(N, M)$and redefine $\hat{\omega}(\lambda)$ such that:

$\hat{\omega}(\lambda) = \frac{\Lambda_i}{\Lambda_i^2 + \lambda} u_i^T v_i \psi^{\text{obs}}$ (2.17)

Where Λ is a singular diagonal matrix, Λ_i denotes a singular value component on the diagonal of the matrix and $uv^T$is a singular vector. In terms of calculation efficiency, the equation after SVD can better reflect the information of the main components, which effectively reduces the amount of calculation. Besides, the selection of the regularization parameter λ is also crucial. This paper uses the L-curve method (logarithmic-logarithmic intersection graph ofϕ_d and ϕ_m) to define the optimal value of the regularization parameter (Hansen, 1998).

2.3 Permeability Estimation

Regarding the description of Vogt et al. (2014), two types of potential field equations are connected by the Darcy velocity formula:

$\sigma \nabla^2 \psi = -\rho\gamma Q_V(K) K \nabla^2 \text{h}$ (2.18)

Among them, the spatial change of the pressure p (Pa) denotes the change of the hydraulic head $p = \rho\gamma\nabla h$. When estimating the permeability K, it is set as an ideal pressure distribution in a uniform half-space. Different pressure distributions can also be applied to the terrain surface or the stratum according to the specific conditions.

$\frac{\sigma \nabla^2 \psi}{\nabla^2 h} = -\frac{\rho\gamma}{}$

english$\mu Q_V(K) K = -\sigma c(K)$(2.19)

$c($ K$)$ denotes the sedimentary coupling coefficient on permeability, which is related to the ratio of potential and pressure and is equal to $\frac{\psi}{h}$. μ is the viscosity of the underground medium. Considering the dependence of$Q_V(K)$ on permeability, we can know:

$\log_{10} \sigma c(K) \mu = -9.2 + 0.18 \log_{10} K$ (2.20)

Combining the above equations, a coupling coefficient value that depends on $K^{0.18}$ can be obtained. Although the permeability dependencies of the coupling coefficient reported in the literature are not as strong as in K (Jardani & Revil, 2009), Vogt et al. (2014) applied it for study to see maximal effects resulting from permeability dependent coupling. The main workflow of SP inversion and permeability estimation is shown in Figure.1.

3 Groundwater Flow Monitoring during a Field Pumping Experiment

3.1 Groundwater Table Hydrological Monitoring

The experiment site is in the hydrological observation site of Jilin University (Figure 2). The ERT survey line is 59 m with an electrode space of 1 m. There are four shallow water wells (C6, Ch2, C1, Ch1), and the pumping test is conducted at the well Ch2.

A standard procedure consists of a continuous pumping for 12 hours at well Ch2. After pumping stops, the groundwater level recovers to the normal within the next 12 hours. Figure 3 visualizes the groundwater level depth in the C6, Ch2, C1, and Ch1 wells along the ERT line. The initial groundwater level is about 2.5 m at 3:30 pm. As pumping water, the depth of the groundwater level in Ch2 declines and reaches a trough value of 6.5 m around 4:50 am (10 hours later). After stopping pump water, the groundwater level slowly returns to the initial depth by groundwater recharge. The water level of wells C6 and Ch1 is slightly changed. The

water level in C1 well shows a significant variation after pumping is stopped. It indicates that the recharging process affects the groundwater level around the well C1.

3.2 ERT Monitoring Test

The 2D ERT time-lapse survey uses the Wenner-Schlumberger array. There are 60 electrodes with an electrode space of 1 m. The recorded apparent resistivity data are inverted using RES2DINV software (Loke, 2006). Figure 4 shows the background ERT result and source current density inverted by SP data before the pumping test. The first low-resistivity layer is about 0˜2.5 m, which corresponds to a high-permeability topsoil layer. The current source density at the same depth also shows high values, which reflects the high flow value in the shallow low-resistance area. It is the natural characteristic of low-resistivity soil. Below 2.5m, it is an unsaturated clay layer. The low resistivity zone in the middle part indicates the groundwater distribution in the shallow well.

The time-lapse ERT surveys last more than 20 hours, and the time interval between subsequent surveys is 1 hour. The recorded data are pre-processed and inverted by the RES2DINV software to obtain the resistivity tomography profile in Figure 5 (left). The time-lapse resistivity tomograms have good consistency, which indicates the reliability of the raw data. Figure 5 (right) is the time-lapse resistivity variation, which is obtained by subtracting ERT results from the background ERT shown in Figure (4). It shows significant spatial and temporal resistivity changes in the pumping area. With the pumping process, the low-resistivity zone gradually becomes deeper. It indicates that the groundwater level declines. Similarly, after pumping water is stopped, the groundwater level steadily recovered, and the low-resistivity at the bottom of the formation increased.

Figure 6 shows the results of resistivity changes over time for wells Ch2 and C1 at different depths. The resistivity changes around the two wells are similar to the hypothetical formation structure. We believe that there are two types of groundwater recharge zones, which have played a key role in different models. In the pumping process, the water level in well Ch2 dominates, and the recharge zone is about 3 m to 6 m. However, the recharge range of well C1 is only 3 m to 4 m, and the resistivity change is consistent with the groundwater level record. In the recovery process, the supply area of well Ch2 is below 6 m, showing a trend from low to high, while the supply range of well C1 is below 4 m, showing a continuous increase in resistivity changes.

3.3 SP Signal Monitoring

The self-potential signal in the pumping test depends on the movement of the groundwater flow. The SP signals are naturally occurring electric field measured at the ground surface with non-polarisable electrodes in the ERT survey line, and the time-lapse interval is 1 hour.

3.3.1 Synthetic Model SP Test

In order to test the SP signal in the pumping process, we first build a synthetic model according to the pumping experiment (Figure 7). The model (50m $\times$ 15m) has three layers. Two drill pipes are set up to simulate the pumping and recovery process. The permeability and conductivity parameters of the model are in Table 1.

A fluid pressure of 1,000 KPa is applied on the surface. Regarding the electrical boundary conditions, Neumann conditions at the surface ensure that potential anomalies can be responded to at the surface. Considering that the bottom permeability of the model is extremely low, and the left and right boundaries are far from the channel, the Dirichlet conditions are given to simulate zero at infinity. The potential underground anomaly obtained through the forward modeling problem is shown in figure 8 (up) and figure 9a. The SP amplitude response has significant changes at different times. It demonstrates that the rise of groundwater has positive self-potential anomalies, while the abnormal negative signals are caused by drawdown. The amplitude of the SP signal decreases with growing distance from the injection well, which roughly matches the prediction of radial flow in a homogeneous medium around an infinite source.

Regarding the inversion problem, the SP signal is used to retrieve the current source density js . A regularization smoothing term is added to the calculation process to solve the ill-posedness of the potential problem. Where calculate the potential field of the jsterm (Cardarelli, 2019), we added the conductivity model used in the forward modeling as a constraint term to invert the potential underground distribution (Figure 9b) and the surface SP signal (Figure 8(bottom)). Comparing the anomalous distributions obtained from the two sets of problems, both can adequately characterize the potential response during the decline and rise of the water level, and the results obtained by the inversion of the water level in the bottom part show instability.

3.3 Time-lapse SP Signal in the Pumping Experiment

The surface SP time-lapse measurements during the pumping test with 1 hour time interval are shown in the left column of Figure 10. It shows a significant SP signal variation during the groundwater flow. The change of the real SP data agrees with the conclusion of the above SP synthetic model test. The SP field shows local negative anomalies during pumping, which is the result of groundwater level decline in the well. When pumping is stopped, the potential anomaly drops significantly and shows multiple positive anomalies, indicating that the water flow in the bottom recharge zone penetrates upwards until the pumping equilibrium.

Using the ERT resistivity as a constraint, we estimate the permeability distribution in the test area according to the SP data (right column of Figure 10). Similarly, the electrical boundary conditions are consistent with those of the forward simulation, and the ground surface uses the Neumann boundary condition. The estimated value of permeability information is a scalar quantity, which represents the information state of groundwater flow sensitivity and distribution in the formation. It can be observed that the characteristics of groundwater flow are evident in the two model phases (pumping and recovery), and they are mainly distributed in the shallow formations around well Ch2.

4 Discussion

The ERT and SP results show reliable evidence to describe the groundwater pumping and recharge experiments. In Figure11a, we compare the time-lapse hydrological groundwater level monitoring at well Ch2 to the ERT and SP results. The groundwater level increases from the initial depth (2.5m) to 6.5 m at the pumping water stage (from 3:30 pm to 6:50 am). Then, the groundwater level returns to the initial depth by the groundwater recharge. Since the soil moisture content reduces in the pumping stage, the resistivity increases to the maximum value of 8.4 Ohm.m (Figure 11b). Then, the resistivity decreases to initial value after the groundwater recharge. It is consistent with the groundwater level change in Figure 11a. There is a positive correlation between the groundwater level and the soil resistivity.

The SP field at the same depth near the wellhead (Figure 11c) has a negative correlation with the groundwater level change. The estimated permeability by SP and ERT coupling coefficient is in Figure 11d. The primary relationship between the permeability and moisture content in unsaturated soil is that the high moisture content corresponds to low permeability (Gómez et al., 2019; Miao et al., 2018). The reason is that increase in water level depth means that the moisture content reduces. Then, the soil porosity will increase with permeability.

The permeability response is not directional, but it shows a derivative change in the water level detection results. The peak value of the pumping period is at 7 pm. The permeability value shows a significant increase with the rapid decline of the water level, and the permeability gradually decreases in the saturated state in the late pumping period. In the same way, within the pumping stops, the rise of the groundwater level causes the permeability to increase. When the water level returns to its original state, the permeability is flat with the background value.

Based on the following discussion, we build the conceptual model to display the groundwater flow characteristics around well Ch2 and well C1 (Figure 12). The process of groundwater flow can be divided into two stages (Figure 12a: pumping and Figure 12b: recovery), and the main layered recharge is concentrated in the changing area of water level. It is clear to see that in the pumping model, the central formation becomes the main recharge area in the well, and in the recovery stage, the deep structure recharges the water to the well.

The continuous recharge zone around well C1 corresponds to the low resistivity zone. It can be interpreted as an area of high permeability and high moisture content, both of which provide groundwater recharge.

5 Conclusion

We combined the time-lapse ERT and SP methods to monitor the dynamics in groundwater flow. Groundwater flow infiltrates and transfers between soil particles and pores, and the moisture content affects the formation and other parameters to some extent. The ERT result establishes linkages between the resistivity and moisture content to reveal the change of groundwater flow. Besides, the SP field is sensitive to the groundwater flow by groundwater dynamics. The rise and drawdown of groundwater will produce positive and negative SP field, respectively. The pumping water experiment results demonstrate that the ERT and SP method combined can provide a reliable way to describe the variation of groundwater flow and understand the qualitative relationship between groundwater flow and its geophysical response.

Data Availability Statement

Data associated with this research are available and can be obtained by contacting the corresponding author.

Acknowledgments

This work are supported by the Natural Science Foundation of China (41874134), the Jilin Excellent Youth Fund (20190103142JH) and the China Postdoctoral Science Foundation 2015M571366

REFERENCES

Bowling, J., Zheng, C., Rodriguez, A., Harry, D., (2006) Geophysical constraints on contaminant transport modeling in a heterogeneous fluvial aquifer. J Contam Hydrol, 85, 72-88

Carey, A.M., Paige, G.B., Carr, B.J., Dogan, M. (2017). Forward modeling to investigate inversion artifacts resulting from time-lapse electrical resistivity tomography during rainfall simulations. Journal of Applied Geophysical, 145, 39–49.

Darnet, M., Maineult A., and Marquis G. (2004). On the origins of self-potential (SP) anomalies induced by water injections into geothermal reservoirs. Geophysical Research Letters, 31 (19), L19609, doi:10.1029/2004GL020922.

Doetsch, J., Linde, N., Vogt, T., Binley, A., and Green, A., (2012). Imaging and quantifying salt-tracer transport in a riparian groundwater system by means of 3D ERT monitoring. Geophysics, 77: B207-B218.

Elédn, L. (1977). Algorithms for regularization of ill-conditioned least squares problems. BIT Numerical Mathematics, 17(2), 134–145.

Fan B, Liu X, Zhu Q, Qin G, Li J, Lin H, Guo L(2020). Exploring the interplay between infiltration dynamics and Critical Zone structures with multiscale geophysical imaging: a review. *Geoderma* , 374:1-16.

Fagerlund, F., Heinson, G (2003). Detecting subsurface groundwater flow in fractured rock using self-potential (SP) methods. Env Geol 43, 782–794.

Gómez Etzar, Broman Viktor, Dahlin Torleif, Barmen Gerhard, Rosberg Jan-Erik. (2019). Quantitative estimations of aquifer properties from resistivity in the Bolivian highlands.H2Open Journal, 2 (1): 113–124. doi:https://doi.org/10.2166/h2oj.2019.007

Guo L, Mount G, Hudson S, Lin H, Levia D (2020). Pairing geophysical techniques improve understanding of the near-surface Critical Zone: visualization and confirmation of preferential routing of stemflow along coarse roots. *Geoderma* , 357:1-12

Hansen, P.C (1998). Rank-Deficient and Discrete Ill-Posed Problems: Numerical Aspects of Linear Inversion. SIAM, Philadelphia p. 247.

Ikard, S. J., Teeple, A. P., Payne, J. D., et al. (2018). New Insights on Scale-dependent Surface and Groundwater Exchange from a Floating Self-potential Dipole. Journal of Environmental & Engineering Geophysics, 23(2), 261-287. doi: https://doi.org/10.2113/JEEG23.2.261

Jardani, A., Revil, A., Barrash, W., Crespy, A., Rizzo, E., Straface, S., Cardiff, M., Malama, B., Miller, C., Johnson, T. (2009). Reconstruction of the water table from self-potential data: a Bayesian approach. Groundwater, 47, 213–227.

Jardani, A., Revil, A., Bolève, A., Dupont, J.P., Barrash, W, Malama, B. (2007). Tomography of groundwater flows from self-potential (SP) data. Geophysical Research Letters, 34, L24403, doi: http://dx.doi.org/10.1029/2007GL031907.

Jongmans, D., Garambois, S. (2007). Geophysical investigation of landslides: a review. Bulletin De La Société Géologique De France, 178, 101–112.

Li, Y., Oldenburg, D.W. (1998). 3-D inversion of gravity data. Geophysics, 63(1), 109–119.

Linde, N., Revil, A., Bolève, A., Dagès, C., Castermant, J., Suski, B., Voltz, M. (2007). Estimation of the water table throughout a catchment using self-potential and piezometric data in a Bayesian framework. Journal of Hydrology, 334(1-2): 88-89. doi: https://doi.org/10.1016/ j.jhydrol.2006.09.027.

Loke, M.H. (2006). RES2DINV Rapid 2-D resistivity and IP inversion using the least-squares method. Geotomo Software, Malaysia.

Menke, W. (1984). Geophysical Data Analysis: Discrete Inverse Theory. Academic Press, p. 289.

Minsley, B. J. (2007). Modeling and Inversion of Self Potential Data. Massachusetts Institute of Technology. Doi:*http://dspace.mit.edu/handle/1721.1/40863*

Naudet,V., Revil, A., and Bottero, J.Y.(2003) Relationship between self-potential (SP) signals and redox conditions in contaminated groundwater. Geophysical Researcg Letters, 30(21), 2091

Nielsen, M. Th. Van Genuchten, Biggar, J. W.(1986). Water flow and solute transport processes in the unsaturated zone, Water Resource Research, 1986, 22(9): 89-108.

Niesner, E. (2010). Subsurface resistivity changes and triggering influences detected by continuous geoelectric monitoring. The Leading Edge, 29(8), 952-955.

Ogilvy, R. D., Meldrum, P. I., Kuras, O., Wilkinson, P. B., Chambers, J. E., & Sen, M., et al.(2009). Automated monitoring of coastal aquifers with electrical resistivity tomography. Near Surface Geophysics, 7(6), 367-376.

Oliveti, I., Cardarelli, E. (2019). Self-Potential Data Inversion for Environmental and Hydrogeological Investigations. Pure and Applied Geophysics, 176, 3607–3628. doi: https://doi.org/10.1007/s00024-019-02155-x

Revil, A., Mendonça, C.A., Atekwana, E.A., Kulessa, B., Hubbard, S.S., Bohlen, K.J. (2010). Understanding biogeobatteries: Where geophysics meets microbiology. Journal of Geophysical Research, Biogeosciences, 115, G00G02. Doi: 10.1029/2009jg001065.

Revil, A., Linde, N., Cerepi, A., Jougnot, D., et al. (2007). Electrokinetic coupling in unsaturated porous media. Journal of colloid & interface science, 313, 315–327.

Sill, W.R. (1983) Self-potential modeling from primary flows. Geophysics, 48, 76–86.

Soueid Ahmed, A., Jardani, A., Revil, A., Dupont, J.P. (2013). SP2DINV: A 2D forward and inverse code for streaming potential problems. Computers and Geosciences, 59, 9-16. Doi: https://doi.org/10.1016/j.cageo.2013.05.008.

Trujillo-Barreto, N.J., Aubert-Vásquez, E., Valdès-Sosa, P.A. (2004). Bayesian model averaging in EEG-MEG imaging. NeuroImage, 21(4), 1300–1319.

Vogt, C., Klitzsch, N., Rath, V. (2014). On self-potential data for estimating permeability in enhanced geothermal systems.Geothermics, 51, 201-213.

Tesfaldet, Y. T., AvirutPuttiwongrak. (2019). Seasonal Groundwater Recharge Characterization Using Time-Lapse Electrical Resistivity Tomography in the Thepkasattri Watershed on Phuket Island. Hydrology, 6(2), 36.

Yanan Miao, Xiangfang Li, Yunjian Zhou, Keliu Wu, Yucui Chang, Zhihua Xiao, Nan Wu, Wenji Lin. (2018). A dynamic predictive permeability model in coal reservoirs: Effects of shrinkage behaviour caused by water desorption. Journal of Petroleum Science and Engineering, 168, 533-541. Doi: https://doi.org/10.1016/j.petrol.2018.05.028

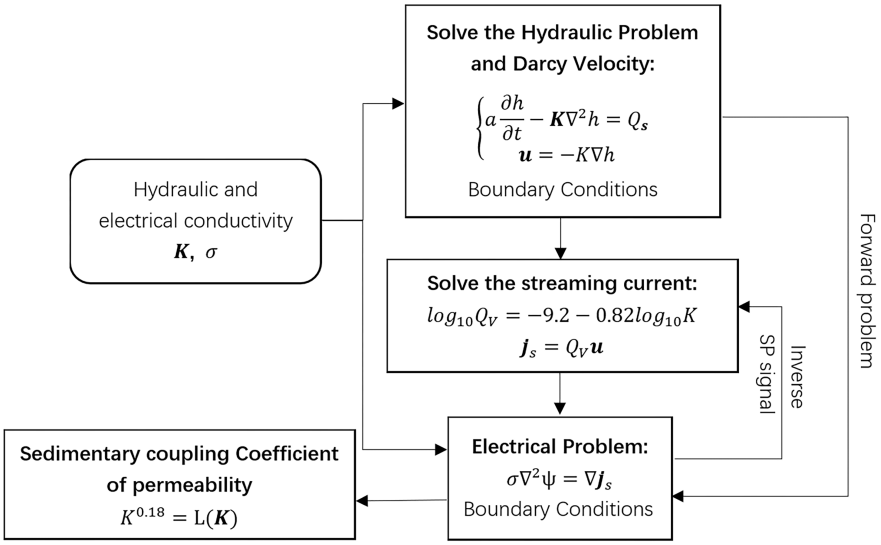

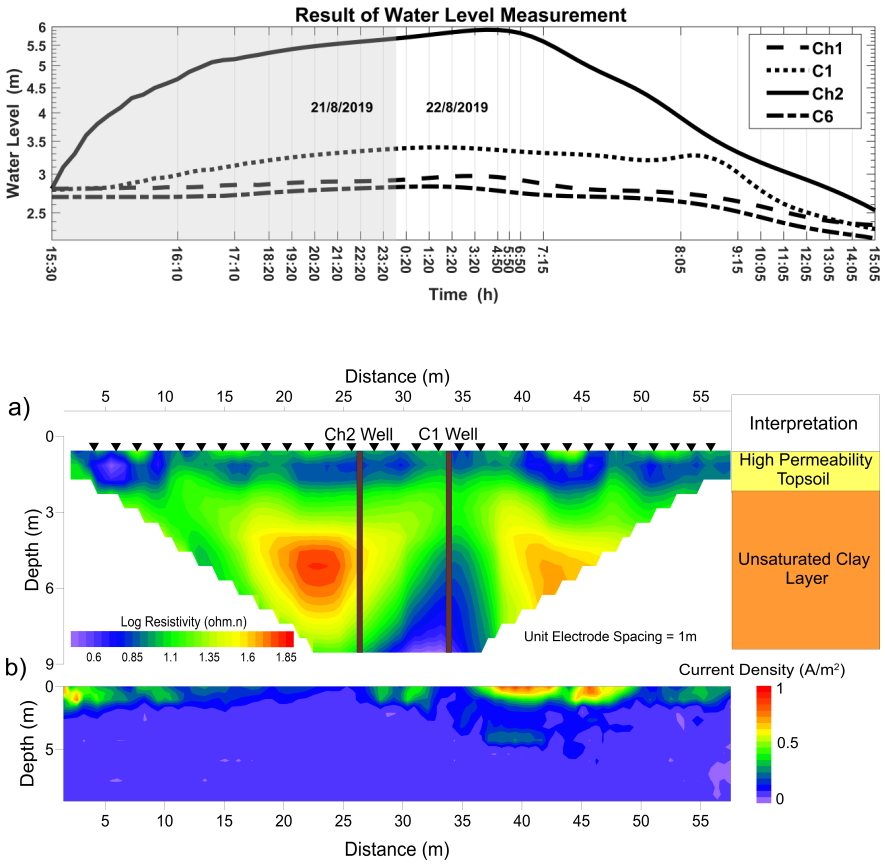

Hosted file

figure5.eps available at https://authorea.com/users/313993/articles/454283-groundwater-flow-monitoring-via-combined-time-lapse-electrical-resistivity-and-self-potential-data-tomography

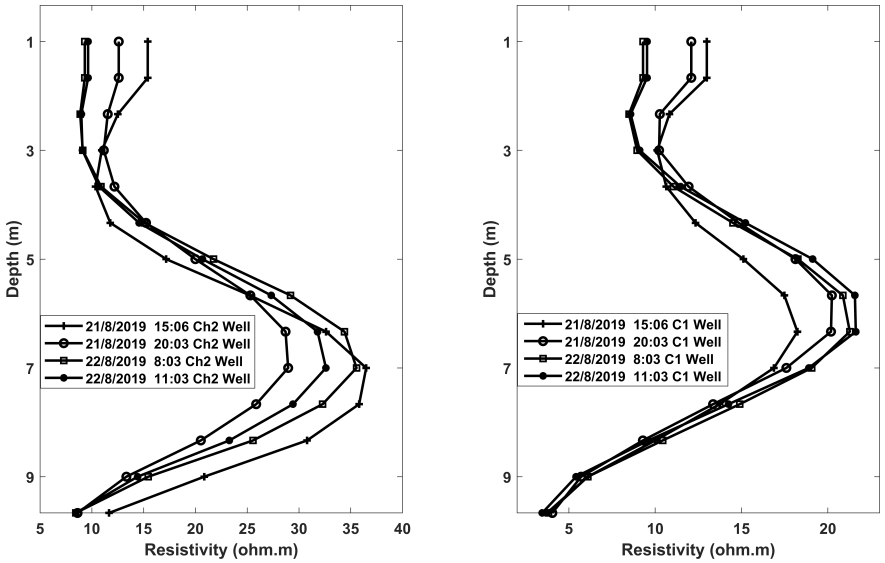

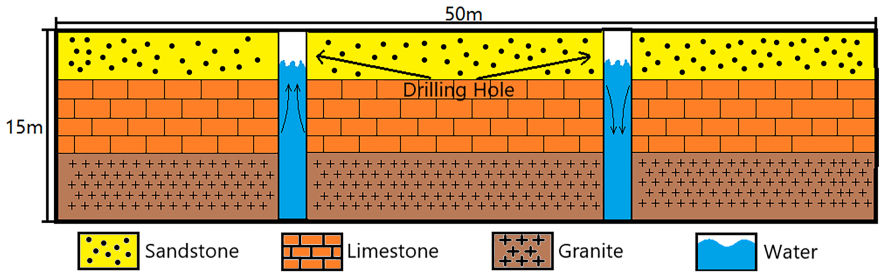

Material	Sandstone	limestone	granite	Permeable conduits
Conductivity (S/m)	0.0067	0.005	0.0025	0.025
Permeability ($\times 10^{-3}$ m^2)	1.0181	1.0176	1.0068	1.0183